JOURNAL OF MATERIALS SCIENCE 7 (1972) 1454–1464

The mechanical properties of carbon fibre reinforced Pyrex glass

D. C. PHILLIPS*, R. A. J. SAMBELL†, D. H. BOWEN*
Atomic Energy Research Establishment, Harwell, Didcot, Berks, UK

The mechanical properties of carbon fibre reinforced Pyrex glass are discussed in terms of the volume fraction of fibre, the orientation of the fibres, fibre damage during fabrication, matrix porosity, matrix critical strain, interface properties and the mode of failure in bend tests. The stress at which matrix cracking occurs increases with fibre concentration indicating that the critical strain of the matrix increases as the fibre separation decreases. The ultimate strength of the composite is considerably greater than the stress at which the matrix begins to crack. Preliminary stress cycling experiments at stresses above that at which matrix cracks are formed suggest that propagation of these cracks is inhibited by the fibres.

1. Introduction

The general principles of the fibre reinforcement of polymers and metals are well established but there has been little verification of the applicability of these principles to ceramics. There are fundamental differences between the three classes of materials which lead to different behaviours under stress. Metals tend to be ductile and polymers have a high compliance so that their failure strains are higher than those of ceramics. The carbon fibre – ceramic matrix system is unusual in that the failure strain of the fibre is higher than that of the matrix, while for most other composites the opposite is true. It is therefore of interest that the carbon fibre – ceramic system should be studied in some detail.

Some of the factors which must be taken into account in the fabrication of carbon fibre reinforced ceramics, and some of the mechanical properties of these materials have been described recently [1-3]. The incorporation of brittle fibres into ceramic matrices can produce a composite ceramic which not only has an increased strength, but also a markedly increased toughness. An unreinforced ceramic has a work of fracture of $\sim 10\ \mathrm{Jm^{-2}}$, while the presence of fibres can increase this value to more than $10^3\ \mathrm{Jm^{-2}}$. This increased toughness is well illustrated by contrasting the fracture behaviour of glass ($\sim 10\ \mathrm{Jm^{-2}}$) and wood ($\sim 10^3\ \mathrm{Jm^{-2}}$), and results in the ceramic having increased impact strength and resistance to thermal shock. Fibre reinforced ceramics are therefore potentially of considerable importance. This paper describes in more detail the mechanical properties of one of those systems, namely carbon fibre reinforced Pyrex glass (CRG).

2. Experimental techniques

Samples were fabricated in graphite dies in air by a hot-pressing technique [2, 3]. There are two main factors that can affect the mechanical properties of material produced in this way. These are matrix porosity and fibre damage. Because of these, different fabrication conditions can lead to different mechanical properties. The work described in this paper was carried out on material which was produced under two different sets of conditions. The data which describe the effect of orientation on strength was obtained from material produced under one set of conditions, but all the other data were obtained from material produced under another set of conditions.

Flexural strengths (σ) and interlaminar shear strengths (τ) were obtained from 3-point bend tests carried out on an Instron machine, assuming the standard beam formulae. Specimens were machined with a diamond saw and tested with their surfaces in the as-cut condition. Their cross-

*Process Technology Division
†Materials Development Division

© 1972 Chapman and Hall Ltd.

TABLE I Microstructure and strength as a function of fibre volume fraction

Volume of fibres (vol %)	Volume of Pyrex (vol %)	Open porosity (vol %)	Closed porosity (vol %)	Porosity as a percentage of matrix (%)	Mean flexural strength (MN/m^2)	Mean maximum shear stress (MN/m^2)	Mean bendover stress (MN/m^2)
22.9	74.2	2.2	0.7	3.8 ± 0.6	410	47	159
23.3	73.9	1.6	1.2	3.7 ± 0.6	480	44	136
29.3	67.1	2.5	1.1	5.1 ± 0.7	560	51	454
40.2	57.3	1.0	1.5	4.2 ± 0.8	680	63	338
51.4	45.7	2.8	0	5.8 ± 1.0	700	71	191
59.5	26.2	14.4	0	35.4 ± 1.5	310	18	247

sections were typically 2.5 × 1 mm and the spans were 40 mm for the bend specimens and 4 mm for the shear specimens. Bending of the long beams was carried out at a cross-head speed of 1 mm/min, and of the shear beams at 0.1 mm/min. Elastic modulus measurements were carried out by an ultrasonic pulse technique and hence at low stresses. Fibre volume fractions and matrix porosities were determined using a combination of density and fibre burn-out measurements [3]. Two types of porosity can exist in the composite, open porosity and closed porosity. The uncertainties in the porosity estimates were quite large because the closed porosity measurement relied on the assumption that all the fibre in the composite could be burned away, and the open porosity measurement relied on being able to fill all the open pores with water by vacuum infiltration. These conditions were difficult to ensure in practice and at best the uncertainties on 1 vol% of open or closed porosities are respectively 0.2 and 0.3 vol% and may be larger.

All the fibre used in this work was the AERE type I high modulus surface treated type with a mean diameter of 8 μm. Fibre strengths were measured by a whole-tow technique and Young's moduli by a single filament method.

3. Results

Table I shows the fibre volume fractions and porosities of a series of compacts made from a single tow under the same hot-pressing conditions. Fig. 1 shows the variation of mean flexural strength with fibre volume fraction, the standard error of each set of six specimens, and the maximum and minimum values of the sets. Fig. 2 shows the maximum shear stresses at failure, calculated from the results of short beam interlaminar shear tests. Table II compares the mean values of flexural strengths and maximum shear

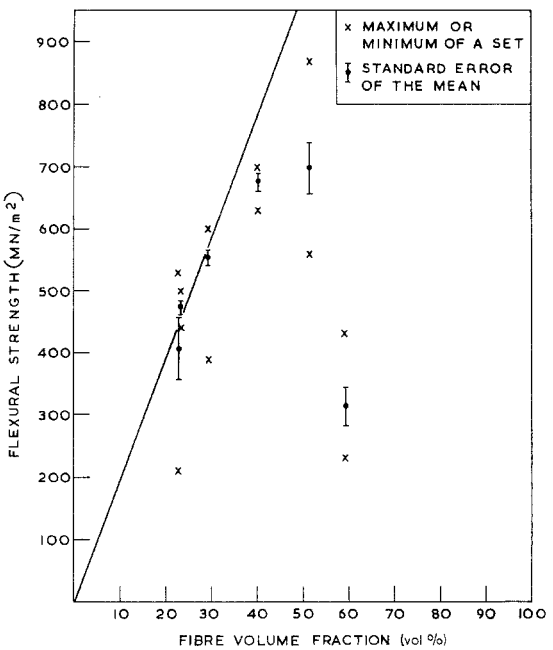

Figure 1 Flexural strength as a function of fibre volume fraction.

TABLE II The σ/τ ratio and calculated and observed loads at failure as a function of fibre volume fractions

Fibre loading (vol %)	σ/τ	Observed short beam failure load (N)	Calculated short beam failure load (N)
22.9	8.7	1.6	1.9
23.3	10.9	1.8	2.2
29.3	11.0	1.7	2.6
40.2	10.8	2.2	3.2
51.4	9.9	2.5	3.2
59.5	17.2	0.6	1.4

stresses obtained from Figs. 1 and 2 and shows that between 23 and 51 vol% the ratio σ/τ seems independent of fibre concentration, lying between

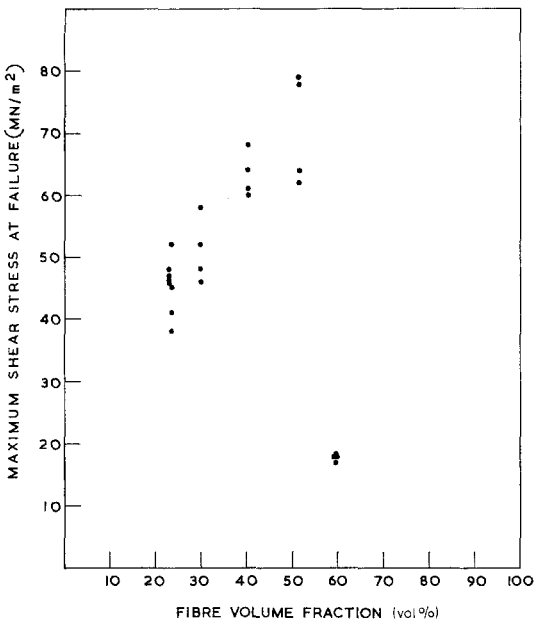

Figure 2 Maximum shear stresses at failure, for a length: depth ratio of 4:1 as a function of fibre volume fraction.

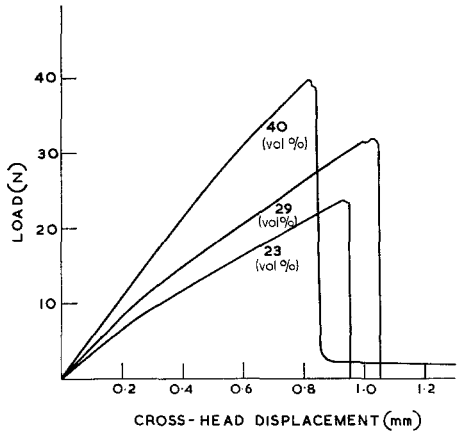

Figure 4 Load versus deflection in 3-point bending for 23, 29 and 40 vol % of fibre.

8.7 and 11.0. The variation of Young's modulus is shown in Fig. 3.

Figs. 4 and 5 show typical load versus deflection curves of long beams in 3-point bending. All the curves are initially linear but bend over at some load considerably less than the maximum, and Table I shows the variation of the mean bendover stress (σ_B) with fibre volume fraction. Increased fibre concentration led to an increasingly controlled failure and the weak, porous, 60 vol% specimen was the most controlled. The load-deflection curve of the 60 vol% specimen shown in Fig. 5 was the only one of the set which did not show an immediate large fall in strength after the maximum load was reached. Similar behaviour was observed in many other specimens and was associated with high fibre concentrations and relatively low flexural and shear strengths. When such a

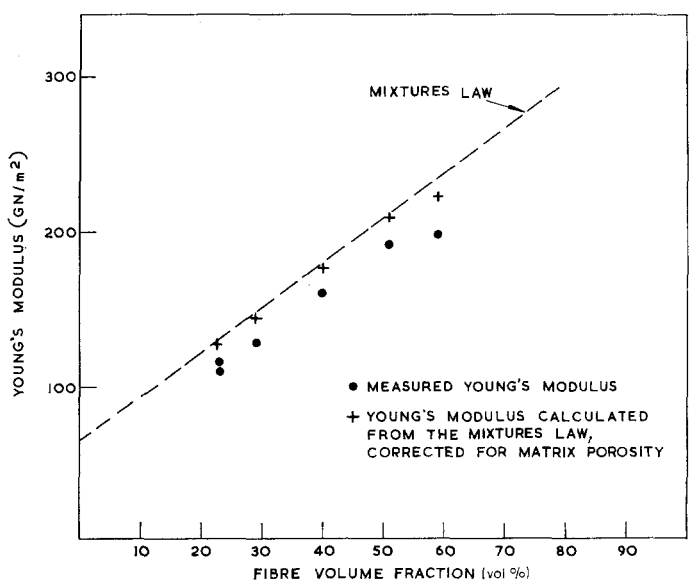

Figure 3 Young's modulus as a function of fibre volume fraction.

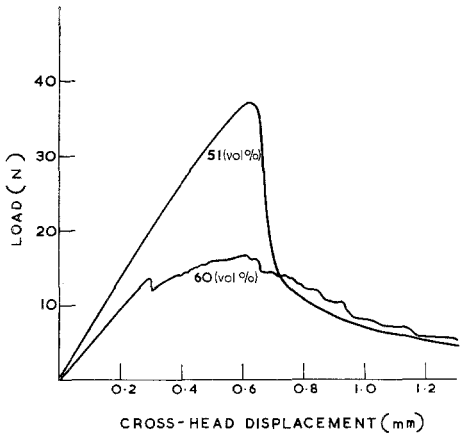

Figure 5 Load versus deflection in 3-point bending for 51 and 60 vol %.

material was loaded beyond its maximum load bearing capacity, the load could be removed and on reapplication could be built up to a value close to that which it bore immediately before removing the load.

A microscopic examination confirmed that fracture of long beams during bending was initiated by failure on the tensile face. The surface microstructure of mechanically polished specimens was studied at different stages of loading to identify the reason for the deviation from linearity. The specimens were loaded to a given stress level,

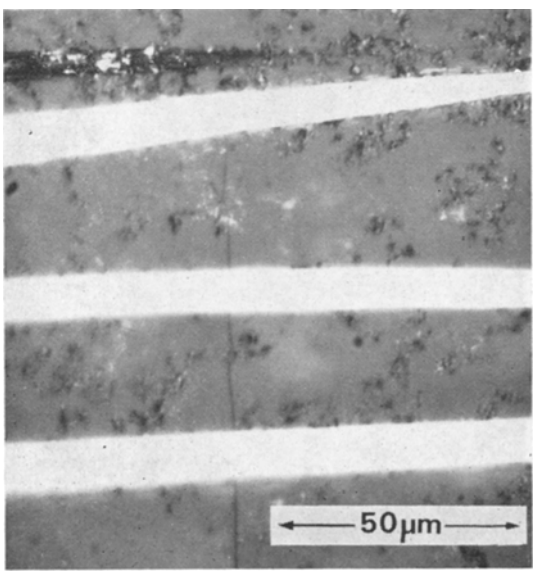

Figure 6 Optical micrograph of the onset of matrix cracking in the tensile face. The crack is localized, ending at the top fibre.

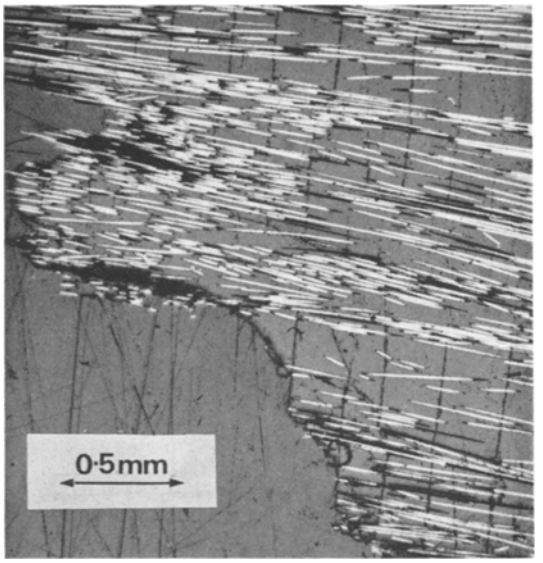

Figure 7 Optical micrograph of a tensile face after complete fracture.

the load was removed and the surfaces examined microscopically. On applying loads lower than that at which bendover occurred no matrix cracking could be observed. At a load where bendover could just begin to be detected, very fine cracking of the matrix was observed in the central region of the tensile face and a photograph of this, in a 22 vol % specimen, is shown in Fig. 6. The cracking was not continuous across the whole width of the tensile face but extended over small regions connecting several fibres, in a direction roughly perpendicular to the tensile stress. As the load was increased, more cracks appeared and occurred further away from the region of maximum tensile stress, existing cracks growing longer and wider. Cracking also became visible in the tensile half of the side face. Figs. 7 and 8 are photographs of the tensile face and a side face in the vicinity of fracture of a different specimen. There are many, regularly spaced cracks running across the tensile face and to the centre of the side face of the specimen. It is clear that multiple fracture of the matrix occurs at stresses well below the ultimate strength of the composite and causes a bendover in the load-deflection curve. Typically the crack spacing is of the order of a few hundred microns.

The effect of cyclic loading into the cracked matrix region was studied in bending in a specimen containing 40 vol % of fibre. The specimen was one of a set of six, the other five of

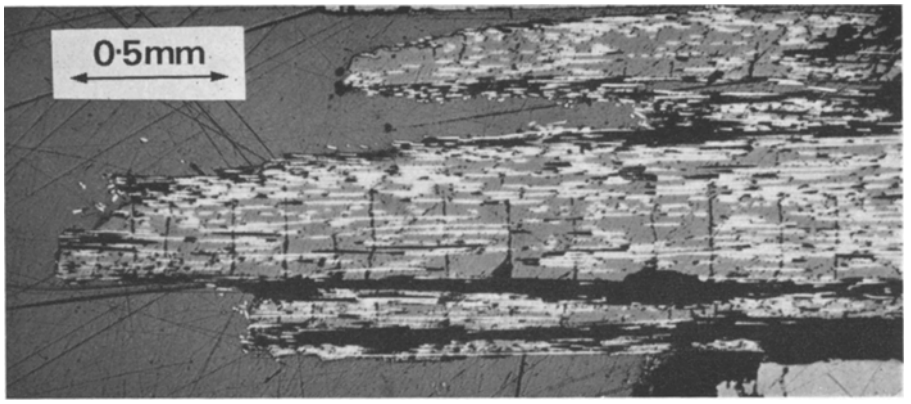

Figure 8 Optical micrograph of a side face after complete fracture.

which had fracture strengths lying between 630 and 700 MN/m², and bendover stresses between 315 and 362 MN/m². Cyclic stressing, at a frequency of 0.4 Hz, was carried out in an Instron machine pre-set to cycle between two fixed gauge positions so that the specimen was bent cyclically between two fixed amounts of deformation. The loads corresponding to these two levels of deformation did not vary during the experiment so that the specimen was also stressed cyclically between two fixed stress levels. The lower stress was negligible and the higher stress was 510 MN/m². Bendover occurred at a stress of 380 MN/m², thus the higher stress was well into the cracked matrix region. On first loading and then unloading, the material underwent a small permanent set, which was illustrated as a hysteresis on the Instron recorder. The unloading part of the loop was essentially linear. On reloading to the same maximum load, the loading and unloading parts were both linear and there was no hysteresis, nor was there a change in shape during the whole experiment. After a total of approximately 22000 cycles, the specimen was loaded to failure and fractured under a stress of 641 MN/m² which is within the spread of strengths of the other five specimens.

Fig. 9 shows the effect of fibre orientation on bend strength. Two types of specimen (A and B) were studied and are shown in Fig. 10. The orientation was measured with respect to the direction of maximum tensile stress and is plotted against the tensile stress in the region where failure occurred rather than the maximum tensile stress. This was necessary because some specimens did not fail at the centre of the bending span. All the specimens were obtained from a single plate with a fibre volume fraction of 48 vol %. Their nominal orientations were 0, 5, 10, 20, 40, 60 and 90°, and two sets of each orientation were tested, the similar sets being obtained from different areas of the plate in order to minimize the effect of local variations in fibre concentration and tow strength. From each of the fourteen sets, five each of types A and B were tested and the strongest and weakest of each group were mechanically polished so that the tensile face and the side face in the vicinity of fracture could be studied. The mean orientation of the fibres was measured by means of a microscope with a calibrated rotating stage. Type A specimens tended to be stronger than type B specimens. Table III shows the mean strengths of each nominal orientation. Ten of the A sets had

TABLE III The mean strengths and nominal orientations of A and B specimens

Nominal orientation	Mean strength (MN/m²)	
	Type A	Type B
0°	340	140
	430	450
5°	550	440
	407	450
10°	360	320
	272	177
20°	110	72
	113	90
40°	35	33
	32	32
60°	24	17
	23	16
90°	6.7	6.7
	14	17

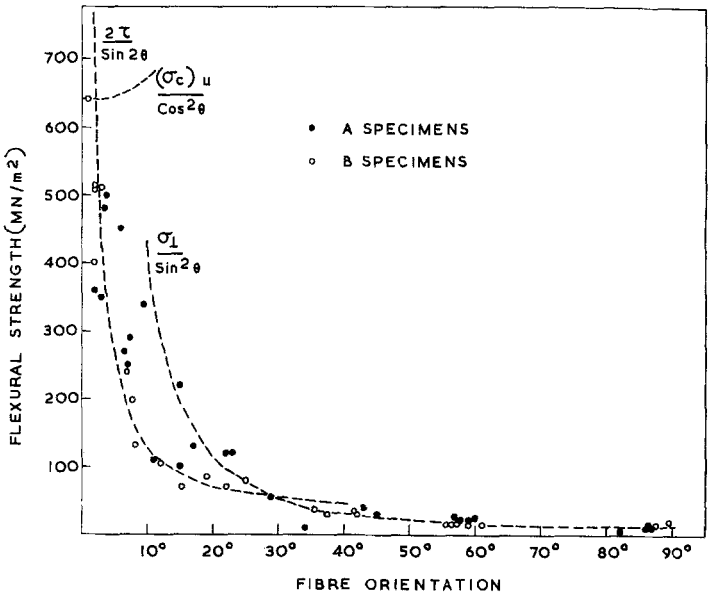

The effect of fibre orientation on flexural strength.

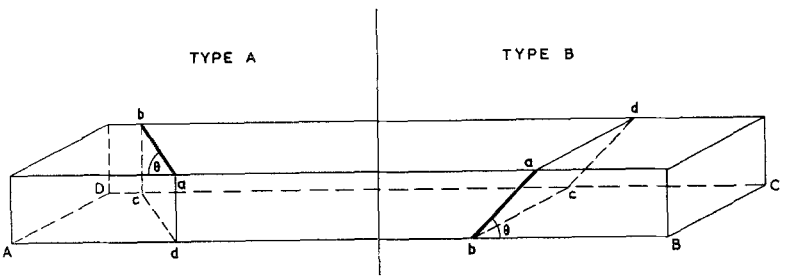

Figure 10 Fibre orientation in A and B specimens. ABCD is the neutral plane of bending. AB is the direction of maximum tensile stress. Fibres lie parallel to ab.

higher strengths than the B sets, one pair of sets was equal and three A sets were weaker than the B sets.

4. Discussion

4.1. The effect of fibre volume fraction

4.1.1. Flexural strength

The observation that fracture commenced by failure on the tensile face showed that it was the tensile properties of the material which were important in bending. For a unidirectional continuous fibre composite in which a tensile load is applied parallel to the fibres, the ultimate tensile strength $(\sigma_c)_u$ is frequently given, to a first approximation, by a mixtures law.

$$(\sigma_c)_u = (\sigma_f)_u V_f + \sigma_m V_m \quad (1)$$

where $(\sigma_f)_u$ is the UTS of the fibres, σ_m is the stress in the matrix when the stress in the fibres reaches $(\sigma_f)_u$, and V_f and V_m are the volumes of fibres and matrix respectively. This is derived by assuming conditions of equal tensile strain in fibres and matrix and that fracture occurs at the failure strain of the fibres. Its main limitations arise because the failure strain of a fibre population is not a unique quantity and because the properties of the fibre-matrix interface can affect the mechanics of failure. The critical strain at which fracture occurs in bulk Pyrex is typically about 1.7×10^{-3} while that of high modulus carbon fibres is about 4.0×10^{-3} so that under conditions of equal tensile strain the matrix is expected to fail before the fibres. The mixtures law then reduces to

$$(\sigma_c)_u = (\sigma_f)_u V_f \quad (2)$$

and the solid line in Fig. 1 represents this theoretical strength of the composite for the measured whole tow strength of 1950 MN/m².

The experimental bend strengths in Fig. 1 have been calculated from the simple beam formula which implicitly assumes that the Young's modulus of the beam material is the same in tension as in compression. The occurrence of matrix cracking during bending leads to a decrease in the Young's modulus of the material in the tensile region. This causes the neutral axis of bending to move towards the compressive face and results in the simple bending beam formula over-estimating the tensile stress. The effect is relatively small – it can be shown to be a few per cent for a 40 vol % specimen – but this emphasizes that the mean strengths began to deviate from the mixtures law above about 30 vol % of fibres and showed a considerable decrease above 51 vol %. At 60 vol % the porosity was considerably greater than at the lower fibre concentrations and this was undoubtedly responsible for the low strength of these specimens. Between 23 and 51 vol % the porosity expressed as a function of the matrix volume varied between 3.7 and 5.8 % and a comparison of Fig. 1 with Table I suggests a correlation between deviation from the volume fraction law and increasing matrix porosity.

4.1.2. Shear strength – the interlaminar shear test

Fig. 2 appears to suggest that the shear strength is a sensitive function of fibre concentration. There are reasons, however, for questioning whether the shear stresses shown in Fig. 2 represent shear strengths, and it is necessary to consider the short beam interlaminar shear test in some detail.

The short beam test is widely used for determining the shear strength of fibre composites because of its experimental simplicity. When a beam is loaded in 3-point bending, tensile, compressive and shear stresses are generated. The maximum tensile stress occurs at the centre of the extended face and in an isotropic elastic material is given to a good approximation by [4]

$$\sigma = \frac{P}{bd}\left(\frac{3}{2}\frac{l}{d} - \frac{2}{\pi}\right) \quad (3)$$

while the maximum shear stress occurs on the neutral plane of bending and has a value

$$\tau = \frac{3}{4}\frac{P}{bd} \quad (4)$$

where P is the applied load, and l, b and d are the beam span, breadth and depth respectively. Several attempts have been made to calculate the equivalent stresses in elastically anisotropic fibre composites. The major effect appears to be on the shear stresses rather than the tensile stresses, but such calculations are still approximate and will not be considered here. Shear failure occurs if the maximum shear stress exceeds the shear strength before the maximum tensile stress exceeds the tensile strength. Ideally shear failure would be easily recognizable on microscopic examination because the specimen would exhibit fracture along the neutral plane or along planes parallel to it. In practice it is sometimes less straightforward to recognize because of contributions to failure from non-shear stresses. The appearance, after fracture, of the short beam specimens of CRG was very different from that of the long beam specimens which had clearly failed in tension. The short beams had at least partly failed in shear because fracture had occurred predominantly along planes parallel to the neutral plane, but their appearance suggested that there was also a contribution from a tensile failure mode. If it is assumed that the short beams fractured in tension rather than shear, under stresses equal to those at failure in the long beams, a simple relationship can be derived between the short beam maximum shear stresses and the long beam maximum tensile stresses by combining Equations 3 and 4 and using the experimental value of $l/d = 4$. This predicts that σ/τ is constant at 7.1, which is close to the observed value. The tensile strength obtained from a long beam test can be used to calculate the load at which tensile failure would occur in the short beams and Table III shows that the calculated loads for tensile failure are only between 25 and 50 % higher than the observed failure loads. Thus, there is doubt that the calculated shear stresses are the shear strengths and Fig. 2 should be regarded as representing lower limits to the shear strengths between 23 and 51 vol %. This conclusion is supported by work [5] on carbon fibre reinforced plastics which showed that short beam shear tests with an l/d ratio of 5:1 are inaccurate at fibre concentrations below about 40 vol %. The accuracy of the short beam test increases with fibre concentrations and it is probable that the measured

maximum shear stresses at the higher fibre concentrations are not very different from the shear strengths. The 59 vol % specimen had a lower shear strength than the other specimens and this was undoubtedly due to its high porosity.

4.1.3. Young's modulus

The Young's modulus of a fibre composite (E_c) under conditions of elastic deformation of fibres and matrix, is also given to a first approximation by the mixtures law

$$E_c = E_f V_f + E_m V_m \qquad (5)$$

where E_f and E_m are the Young's moduli of fibre and matrix respectively. This expression gives strictly the lower bound of the composite modulus and more exact theories applied to idealized systems predict slightly larger values [6].

Fig. 3 shows that Young's modulus increased linearly with fibre volume fraction between 23 and 51 vol% but deviated from linearity at 59 vol%. On the same diagram is plotted the theoretical variation based on Equation 5 and assuming a constant matrix modulus of 64 GN/m² and a measured fibre modulus of 353 GN/m². In general, the matrix modulus differs from that of fully dense Pyrex because of porosity, and a correction has to be made to the theoretical value. This has been carried out by assuming a relationship between matrix modulus and porosity due to Mackenzie [7]:

$$E_m = (E_m)_0 (1 - 1.9p + 0.9p^2) \qquad (6)$$

where $(E_m)_0$ is the modulus in the absence of porosity and E_m is the modulus in the presence of a total porosity p. This correction has little effect between 23 and 51 vol % but is significant at 59 vol % and suggests that the deviation from linearity of the 59 vol % specimen is due to matrix porosity. Between 23 and 51 vol % the variation of modulus is parallel to the prediction of the mixtures law but smaller than the theoretical value by about 20 GN/m². Reynolds [8] has shown that the Young's modulus of a carbon fibre decreases rapidly with angle to the fibre axis. Between 0 and 15° it decreases logarithmically by an order of magnitude. It is therefore most probable that the modulus of the present samples was decreased below its theoretical value by the lack of perfect alignment among the fibres.

4.2. Matrix cracking

4.2.1. The strength of the matrix

The stress in the composite (σ_B) at which cracking occurs can be related to the UTS of the matrix $(\sigma_m)_u$ by an extension of Equation 1.

$$\sigma_B = (\sigma_m)_u \left\{1 + V_f \left(\frac{E_f}{E_m} - 1\right)\right\} \qquad (7)$$

The stresses in the matrix at bendover, due to the applied load, have been calculated from Equation 7, assuming a matrix modulus which varies with porosity according to Equation 6. The matrix exists under a state of tension parallel to the fibres, even when the composite is unloaded, due to the differential thermal contraction of matrix and fibres on cooling after hot-pressing [2, 3] and these stresses have been calculated approximately from the simple formula

$$\sigma_m = \frac{(\alpha_m - \alpha_f) E_f V_f \Delta T}{1 + V_f \left(\frac{E_f}{E_m} - 1\right)} \qquad (8)$$

where α_m and α_f are the thermal expansion coefficients of matrix and fibres respectively and ΔT is the difference between the strain point temperature of Pyrex glass and room temperature. This expression is only approximate as it treats the problem as one dimensional. In CRG, the fibres shrink away radially from the matrix on cooling [2] and radial stresses are therefore expected to be negligible. Equation 8 is then expected to give a good approximation to the tensile stresses parallel to the fibres in the matrix, and these have been calculated using the values $\Delta T = 500°C$; $\alpha_m = 3.3 \times 10^{-6}\ °C^{-1}$; α_f in this temperature range was assumed to be $-0.4 \times 10^{-6}\ °C^{-1}$ and E_f was 353 GN/m^{-2}. The matrix strength is the sum of the stress calculated from Equation 7 and that obtained from thermal mismatch and all three are shown as a function of fibre volume fraction in Fig. 11.

The strength of hot-pressed Pyrex glass, in the absence of fibres, is typically about 100 MN/m², while the derived matrix strength increases from 140 MN/m² at 23 vol % to a maximum of 260 MN/m² at 30 vol % and then decreases with increasing fibre concentration to a minimum of 80 MN/m². In unreinforced Pyrex, the growth of a single flaw and its propagation as a crack can result in total failure. The presence of fibres clearly influences the growth and propagation of cracks because cracks are observed to be localized during the early stages of matrix cracking. The increased strength of the matrix suggests that the presence of the fibres also inhibits the initiation of cracks. Recently, Cooper and Sillwood [9] have proposed a theory to

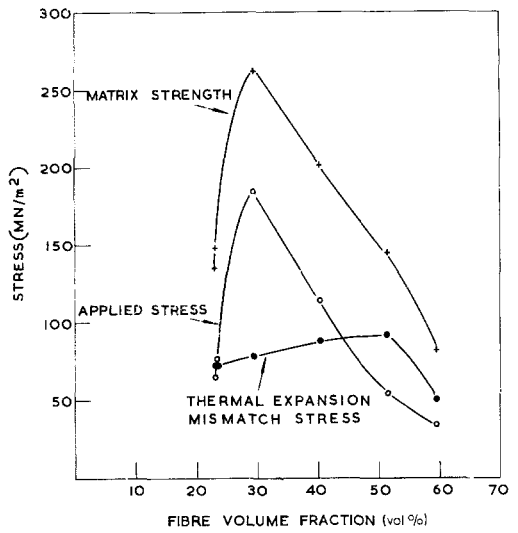

Figure 11 Matrix stresses at bendover, as a function of fibre volume fraction.

explain the increase in strength of a matrix in the presence of fibres. Aveston, Cooper, and Kelly [10] have applied this theory to data obtained from several different materials, including the data presented here, and have found good agreement between theory and experiment. It is not clear why the matrix strength should be a maximum at 30 vol % of fibres, but a possible explanation is that the strengthening effect at increasing fibre volume fractions is opposed by the associated increasing porosity. This would result in the matrix strength reaching a maximum at some fibre concentration.

4.2.2. The shear strength of the interface

The mean separation (t) between matrix cracks can be used to estimate a lower bound for the shear strength (τ_i) of the fibre-matrix interface using the inequality

$$\tau_i > \frac{(\sigma_m)_u r}{2t} \frac{(1 - V_f)}{V_f}$$

which is derived in an Appendix. A 22 vol % specimen with a matrix tensile strength $\sim$ 150 MN/m² displayed a mean crack separation $\sim$ 400 μm, indicating that $\tau_i > 4$ MN/m².

An upper bound for τ_i can also be obtained from an examination of fibres protruding from the fracture face of a discontinuous fibre composite, since in that case [6]

$$\tau_i < \frac{(\sigma_f)_u r}{2l_f} \qquad (9)$$

where l_f is the maximum length of protruding fibre. In [2] it was shown that $l_f \sim 150$ μm so that for a typical value of $(\sigma_f)_u$ of 2000 MN/m², $\tau_i < 27$ MN/m². This value, however, depends on an accurate knowledge of $(\sigma_f)_u$ and, because of the dependence of $(\sigma_f)_u$ on fibre length, this upper bound should be regarded as rather approximate.

4.3. Stress cycling

As this is a single result, it cannot be conclusive. It does, however, indicate that matrix cracking does not produce a markedly deleterious effect on strength under cyclic conditions.

4.4. Orientation effects

Uniaxially aligned fibre composites, under the action of a tensile stress applied to an angle θ to the fibre direction generally fail by one of three mechanisms [6]. These are:

(*a*) failure in a plane perpendicular to the fibres due to tensile failure of the fibres, in which case the fracture stress of the composite is

$$\frac{(\sigma_c)_u}{\cos^2\theta}$$

(*b*) shear failure in a plane parallel to the fibres in which case the fracture stress is

$$\frac{2\tau}{\sin 2\theta}$$

and

(*c*) failure in a plane parallel to the fibres due to tensile failure of the matrix in the unreinforced direction perpendicular to the fibres, resulting in a fracture stress $\sigma_\perp/\sin^2\theta$ where $\sigma_\perp$ is the fracture stress of the composite under a tensile stress applied perpendicular to the fibre direction (transverse tensile strength).

For a given fibre orientation the lowest fracture stress derived from these formulae gives the strength of the material. Fig. 9 shows that strength is clearly a sensitive function of fibre orientation at low angles, and a good agreement is obtained with the theoretically predicted variation. The tensile strength in the direction of the fibres has been taken as the highest measured flexural strength, the shear strength has been obtained from short beam measurements of 0° specimens, and the transverse tensile strength has been taken as the flexural strength of 90° specimens. Between 0 and about 5°, although the strengths fall on the shear failure curve, the microscopic appearance of the specimens revealed

that failure was due primarily to tensile failure. The scatter in strengths at these low angles is essentially a reflection of the scatter in tensile strength. The apparent agreement between the data and the shear failure criterion is a result of this scatter combined with the uncertainty in mean fibre orientation which results from the spread in fibre orientation in a specimen. Between 5 and 30° the strengths are scattered between the shear failure curve and the transverse tensile failure curve. Shear failure in this case should not be confused with short beam shear failure of 0° material where fracture occurs along planes parallel to the neutral plane of bending. In these long beam specimens fracture occurs along the planes marked a, b, c and d in Fig. 10 and is a result of shear stresses arising from the resolved component of the maximum tensile stress in the beam. It is not obvious from an examination of these intermediate-angle specimens whether fracture occurred by shear failure or transverse tensile failure because separation occurs along the same planes in each case. Although theory predicts that at angles lower than 30° failure should occur by shear rather than by transverse tensile fracture, local fluctuations in the properties of the bend specimens alter the shear and transverse strengths from the mean values used to calculate the theoretical curves and complicate the analysis. At angles greater than 30° the agreement between the measured strengths and the transverse tensile failure curve, together with the microscopic appearance of failure, indicates that fracture is due to this mechanism.

The wide scatter of the low angle (< 5°) tensile strengths is a reflection of the generally poor properties of the particular plate from which the specimens were obtained. Fabrication of the plate was not carried out under the best conditions because these had not been established at the time of this experiment. However, it is clear that increased shear strength and transverse tensile strength will decrease the orientation dependence of the flexural strength.

4.4.1. The tensile strength of the interface

The very low strength of the 90° specimens are consistent with a fibre-matrix interface of low tensile strength. On a model in which the interface involves only mechanical keying, and where radial shrinkage of the fibre away from the matrix occurs on cooling during fabrication [2], the interfacial tensile strength is expected to be zero. The transverse tensile strength of the composite will then be that of the equivalent volume of Pyrex containing cylindrical voids. Typically the strength of Pyrex is 100 MN/m². Reducing the volume of glass by the 48 vol % occupied by the fibres reduces the composite strength to 52 MN/m², while the stress concentrating effect of a circular cross-section cylinder is a factor of 3 which further reduces the composite strength to 17 MN/m². This compares reasonably well with the mean measured 90° strength of 12 MN/m².

Acknowledgements

The authors gratefully acknowledge the assistance of several of their colleagues at Harwell. In particular they wish to thank Dr G. J. Curtis of the NDT Centre for carrying out elastic modulus measurements on the composites, and Mr P. R. Goggin of Metallurgy Division for supplying the fibre strength and modulus data.

Appendix

The relationship between interfacial shear strength and multiple matrix cracking

Fig. 12 represents a cross-section through a composite in a region where the matrix has cracked. On plane AB the load is supported by the fibres alone, while on plane CD it is supported by fibres and matrix. Considering only stresses parallel to the fibres, the forces on plane AB equal those on CD and

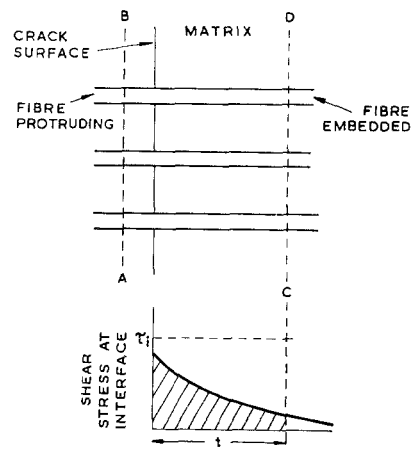

Figure 12 Stresses in fibres and matrix during multiple cracking.

$$V_f(\sigma_f)_{AB} = V_f(\sigma_f)_{CD} + V_m(\sigma_m)_{CD} \quad \text{(i)}$$

where $(\sigma_f)_{AB}$ is the stress in the fibres on plane AB, and $(\sigma_f)_{CD}$, $(\sigma_m)_{CD}$ are the stresses in fibres and matrix respectively on plane CD.

The shear stress variation along the fibre-matrix interface has some general form as shown in Fig. 12. Thus, considering a single fibre, of radius r, at AB and CD.

$$(\sigma_f)_{AB}\,\pi r^2 = (\sigma_f)_{CD}\pi r^2 + k\tau_i\,2\pi rt \qquad \text{(ii)}$$

where k is the ratio of the shaded area in Fig. 12 to $t\tau_i$, τ_i is the interface shear strength, t is the distance between matrix cracks.

Matrix cracking will occur on plane CD when $(\sigma_m)_{CD}$ equals $(\sigma_m)_u$, the UTS of the matrix. Combining (i) and (ii)

$$\tau_i = \frac{(\sigma_m)_u\,V_m\,r}{k\,2t\,V_f} \qquad \text{(iii)}$$

and since $V_m + V_f = 1$ and $k < 1$.

$$\tau_i > (\sigma_m)_u \frac{(1 - V_f)}{V_f}\frac{r}{2t} \qquad \text{(iv)}$$

References

1. D. H. BOWEN, D. C. PHILLIPS, R. A. J. SAMBELL, and A. BRIGGS, "Carbon Fibre Reinforced Ceramics, Proceedings of an International Conference on the Mechanical Behaviour of Materials, Kyoto, Japan, August 1971.
2. R. A. J. SAMBELL, D. H. BOWEN, and D. C. PHILLIPS, *J. Mater. Sci.* 7 (1972) 663.
3. R. A. J. SAMBELL, A. BRIGGS, D. C. PHILLIPS, and D. H. BOWEN, *J. Mater. Sci.* 7 (1972) 676.
4. See, for example, S. TIMOSHENKO and J. N. GOODIER, "Theory of Elasticity" (McGraw-Hill Book Co Inc, Maidenhead, 1951).
5. N. L. HANCOX, AERE-R6225, 1969.
6. See, for example, A. KELLY, "Strong Solids" (Clarendon Press, Oxford, 1966).
7. J. K. MACKENZIE, *Proc. Phys. Soc.* **B63** (1950) 2.
8. W. N. REYNOLDS, 1970, Society of Chemical Industry, 3rd Conference on Industrial Carbons and Graphite.
9. G. A. COOPER and J. M. SILLWOOD, *J. Mater. Sci.* 7 (1972) 325.
10. J. AVESTON, G. A. COOPER, and A. KELLY, 1971, National Physical Laboratory Conference on The Properties of Fibre Composites.

Received 24 April and accepted 11 May 1972.